The effect of potassium chloride on $BiVO_4$ morphology and photocatalysis

Sopheak Meng*, Takaya Ogawa, Hideyuki Okumura, Keiichi N. Ishihara*

Graduate School of Energy Science, Kyoto University, Kyoto 606-8501, Japan

Abstract

The monoclinic $BiVO_4$ was synthesized via a facile one-pot hydrothermal synthesis. KCl concentration in the precursor greatly influences the crystal growth, morphology, and absorption properties of $BiVO_4$ attributed to the effect of Cl^- ions on the formation of BiOCl intermediate and preferential growth of $BiVO_4$ crystals along {010} planes. The photocatalytic property of $BiVO_4$ is accordingly altered based on the KCl content. The "shuriken-like" $BiVO_4$ prepared with 3 mmol of KCl exhibits the highest photocatalytic activity among our samples. Its photocatalytic rhodamine B degradation efficiency could reach 94.7% after 4 h of visible-light irradiation. The degradation efficiency only decreased to 90.8% after four runs of four-hour irradiation. The photodegradation rate with the shuriken-like $BiVO_4$ is around 2.3 times higher than that with the rod-like $BiVO_4$ prepared without KCl, owing to its highest relative intensity ratio of (040) to $(\bar{1}21)$ plane, which maximizes the exposed active {010} facets of $BiVO_4$.

Keywords: Visible-light photocatalyst; KCl; Shuriken-like $BiVO_4$; Morphology

*Corresponding author.

E-mail: sopheak@social-system.energy.kyoto-u.ac.jp (S.Meng); ishihara@energy.kyoto-u.ac.jp (K. N. Ishihara)

1. Introduction

Over past decades, bismuth vanadate ($BiVO_4$) has become one of the most widely-studied photocatalysts ascribed to its favorable properties such as nontoxicity, low cost, narrow bandgap (E_g~2.4 eV), and stability [1]. As a photocatalyst, $BiVO_4$ has been known for its usage in the degradation of organic pollutant [2–4] and oxygen evolution in water splitting [5,6]. Of all three existing phases of $BiVO_4$, only monoclinic scheelite $BiVO_4$ is commonly used due to its superior photocatalytic performance compared with tetragonal scheelite and tetragonal zircon-type counterpart [7–9]. Besides the crystal phase of $BiVO_4$, morphology has a significant impact on the photocatalytic activity of $BiVO_4$ as well.

It has been reported that increasing exposed {010} facets links to a remarkable enhancement of the photocatalytic activity of $BiVO_4$ [2,10–13]. Synthesis techniques involving a structure-directing agent such as $TiCl_3$ [6], NaCl [12,14,15], ammonium carbonate [2], ethylenediamine [3], and glycerol [16] can be used to promote the exposure of {010} facets of $BiVO_4$ through preferential growth of crystals along {010} planes. These studies have indicated a strong relationship between the improvement of photocatalytic performance and the increase in the exposed {010} facets.

Among the directing agents, both $TiCl_3$ and NaCl contain Cl^-, which has been reported to be responsible for stabilizing {010} facets and inducing preferential crystal growth along the {010} plane [15]. However, some metal chlorides, such as $AlCl_3$, CuCl, $ZrCl_4$, and $FeCl_2$, have no notable effect on {010} facets [6]. It may be due to the synthetic condition or the concentration of Cl^- in the solution. Interestingly, some research using $BiCl_3$ as a Bi^{3+} source for $BiVO_4$ preparation has also demonstrated the enhanced exposed {010} facets of $BiVO_4$ [5,11]. The $BiCl_3$ has been widely used to fabricate different morphologies of $BiVO_4$ (nanoplates or nanosheets) [5,11,17,18]. Although $BiCl_3$ contains Cl^- ions, the synthesis route of $BiVO_4$ may be different from the one with Cl^- ions

introduced at later stages of preparation as a directing agent. The order of adding Cl^- ions into the precursor solution could determine the intermediate phase followed by transforming to monoclinic $BiVO_4$. The BiOCl intermediate may occur if Cl^- ions are added before VO^{3-} ions [19,20], while the tetragonal zircon-type $BiVO_4$ would form due to its low formation temperature [7,9,21] if Cl^- ions are added after VO^{3-} ions [6,15]. Nevertheless, few studies have focused on the effect of Cl^- concentration influencing the formation of BiOCl intermediate during the hydrothermal synthesis, which has a significant role in $BiVO_4$ photocatalysis via crystal growth and morphology.

In this study, $BiVO_4$ is synthesized via one-pot hydrothermal synthesis, in which KCl is used as a source of Cl^- ions. Although KCl was used in the $BiVO_4$ synthesis to compare with NaCl in the previous report [15], the effect of KCl on $BiVO_4$ has not been thoroughly studied yet. Thus, the present study investigates and discusses the effect of KCl concentration on the $BiVO_4$ synthesis route, morphology, crystal structure, photocatalytic activity, and other properties. Rhodamine B (RhB) is selected as a model dye to evaluate the photocatalytic performance of each sample because it represents one of the most common organic dyes in textile industry and industrial wastewater [22–25]. The $BiVO_4$ prepared with 3 mmol of KCl, exhibiting "shuriken-like" morphology, demonstrates a superior photocatalytic degradation of RhB dye under visible light illumination because of the enhanced exposed {010} facets and the narrow bandgap.

2. Experimental

2.1. Materials

All chemicals with analytical grade were used without further purification. Bismuth (III) nitrate pentahydrate ($Bi(NO_3)_3 \cdot 5H_2O$, 99.5%), ammonium vanadate (NH_4VO_3, 99.0%), and ethanolamine (2-aminoethanol, C_2H_7NO, ≥ 97.0%) were supplied by Nacalai Tesque (Kyoto, Japan). Potassium chloride (KCl, 99.5%) was purchased from FUJIFILM Wako Pure Chemical Corporation (Osaka,

Japan). The rhodamine B ($C_{28}H_{31}ClN_2O_3$, > 95%) was purchased from Tokyo Chemical Industry (Tokyo, Japan). Direct-Q water purification system (Millipore) was used to obtain ultrapure water for synthesis.

2.2. Preparation of $BiVO_4$ samples

$BiVO_4$ was synthesized via hydrothermal synthesis. Briefly, 0.485 g of $Bi(NO_3)_3 \cdot 5H_2O$ (1 mmol) was hydrolyzed in 30 ml of ultrapure water, and magnetically stirred for 5 min. Then, a certain amount of KCl (0, 1, 2, 3, and 5 mmol) was added to the solution to form a white suspension (slightly soluble BiOCl). After 2 min of stirring, 117 g of NH_4VO_3 (1 mmol) was put into the white suspension, whose color then turned yellowish orange. The pH of the suspension was adjusted to 1.8 using ethanolamine. The suspension remained under stirring for 1 h and agitated under ultrasonication (45 Hz) for another 1 h. Then, it was transferred to 50 ml stainless-steel autoclave with a Teflon liner, which was heated in an electric oven at 160 °C for 12 h. After the heat treatment, the autoclave was allowed to cool down to room temperature. The $BiVO_4$ samples were collected and washed several times with ultrapure water and ethyl alcohol. They were then dried at 90 °C overnight. The samples were labeled as Bi0, Bi1, Bi2, Bi3, and Bi5 based on the amount of KCl content used during the synthesis. The schematic illustration of the preparation procedure can be seen in Fig. S1 (Supplementary Information).

2.3. Characterization

The crystal phase of the sample was determined using X-ray diffraction (XRD) diffractogram obtained from a Rigaku RINT2100 with Cu Kα radiation (λ = 1.5418 Å). Microstructures and morphologies of each sample were investigated using an FE-SEM (Hitachi SU6600 Scanning Electron Microscope) operated at 20 kV, where Au was sputtered on all samples prior to the analyses. UV-vis diffuse reflectance spectra (DRS) were obtained using a Lambda 750S UV/Vis/NIR

Spectrophotometer equipped with a 60 mm integrating sphere. X-ray photoelectron spectroscopy (XPS, JPS-9030 X-ray photoelectron spectrometer) was conducted with Mg Kα radiation using O 1s = 530.0 eV as reference. The Brunauer–Emmett–Teller specific surface area (S_{BET}) of the samples was measured via the single-point BET method using N_2 gas adsorption with a Flowsorb III 2305 Micromeritics instrument (Shimadzu, Japan).

2.4. Photocatalytic measurement

Evaluation of photocatalytic activity was conducted via the photodegradation of rhodamine B (RhB) dye under visible light irradiation. A 500 W Xe lamp (Ushio, UXL-500D-O) with a cutoff filter ($\lambda > 420$ nm) was used to illuminate the RhB solution at room temperature (25 °C). A Spectroradiometer (S-2440 model II) was used to calibrate the light intensity of the Xe lamp to obtain 100 mW/cm^2. The sample solution then received around 40 mW/cm^2 of light intensity due to the cutoff and water filter. For each photocatalytic measurement, 40 ml of RhB solution (0.01 mmol L^{-1}) that contained 30 mg of photocatalyst was poured in a 100 ml capacity beaker. Before light irradiation, the solution in the dark was agitated under ultrasonication for 10 min and magnetically stirred for another 50 min to achieve adsorption-desorption equilibrium between the photocatalyst and RhB solution. During the irradiation, 3 ml of RhB solution was sampled every 60 min intervals and filtered to remove the photocatalyst powder with a syringe filter (0.22 µm, PTFE) prior to the analysis using the Lambda 750S UV/Vis/NIR Spectrophotometer.

3. Results and Discussion

3.1. Crystal structure of the samples

Fig. 1 shows XRD patterns of $BiVO_4$ with different concentrations of KCl. All the samples exhibit characteristic peaks of monoclinic $BiVO_4$ (ICDD PDF No. 00-014-0688), especially, the split peaks at 18.5° and 35°, which are often used to distinguish between tetragonal and monoclinic

phases. It is also noticeable that the intensity of the peak at 30.5°, corresponding to (040) plane of $BiVO_4$, becomes more intense as the amount of KCl is increased. To make a comparison, the relative intensity ratio of (040) to ($\bar{1}21$) plane ($I_{(040)}/I_{(\bar{1}21)}$) for each sample was calculated (Table 1). The $I_{(040)}/I_{(\bar{1}21)}$ intensity ratio rises from 0.46 to 2.46 as KCl concentration is increased from 0 to 3 mmol, while it decreases when KCl content reaches 5 mmol. It demonstrates that the addition of KCl influences the preferential growth of $BiVO_4$ crystals along {010} planes. A previous study using NaCl as a directing agent reported that Cl^- anions played an important role in stabilizing and controlling the exposed {010} facets [15]. A similar result was also reported if the synthesis utilized $TiCl_3$ [6].

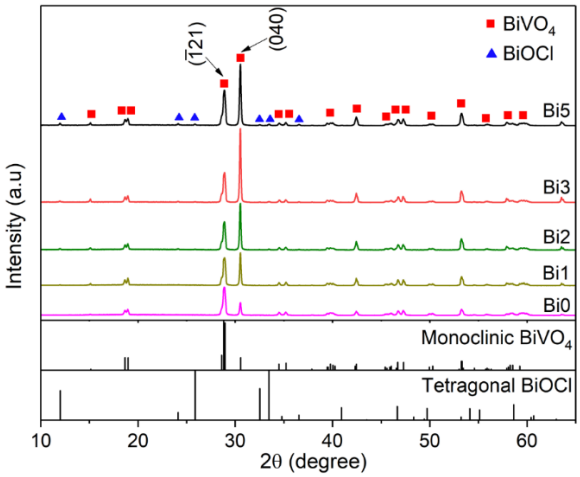

Fig. 1. XRD patterns of $BiVO_4$ with a different amount of KCl (mmol).

Table 1 Relative intensity ratio, physical properties and photocatalytic performance of $BiVO_4$ with a different amount of KCl.

Sample	$I_{(040)}/I_{(\bar{1}21)}$	E_g (eV)	S_{BET} ($m^2\ g^{-1}$)	RhB degradation efficiency (%)	k ($\times10^{-3}\ min^{-1}$)	k/S_{BET} ($\times10^{-2}\ min^{-1}/m^2\ g^{-1}$)
Bi0	0.46	2.48	2.8	70.1	5.03	0.18
Bi1	1.17	2.45	1.1	81.7	6.60	0.60
Bi2	1.68	2.43	0.84	93.4	10.2	1.2
Bi3	2.46	2.34	0.63	94.7	11.4	1.8
Bi5	1.72	2.38	0.51	63.9	4.75	0.93

The additional content of KCl not only affects the crystal growth of $BiVO_4$ but also produces another phase in the samples, as seen in Fig. 1. The small peaks at 12°, 24.1°, 25.9°, 32.5°, 33.5, and 36.5° can be assigned to (001), (002), (101), (110), (102), and (003) plane diffraction of tetragonal BiOCl (ICDD PDF No. 00-006-0249), respectively. These peaks become more visible in samples with higher KCl concentration. The BiOCl could be an intermediate material before the growth of $BiVO_4$ crystals. A possible chemical reaction can be expressed as follows [19,20]:

$$Bi^{3+} + 2H_2O \rightleftharpoons BiOH^{2+} + H_3O^+ \quad (1)$$

$$BiOH^{2+} + H_2O \rightleftharpoons BiO^+ + H_3O^+ \quad (2)$$

$$BiO^+ + Cl^- \rightleftharpoons BiOCl\downarrow \quad (3)$$

$$BiOCl\downarrow + VO_3^- \rightleftharpoons BiVO_4\downarrow + Cl^- \quad (4)$$

The synthetic reaction begins with hydrolysis of $Bi(NO_3)_3{\cdot}H_2O$ [reaction (1) and (2)]. The BiO^+ derived from hydrolysis reacts with Cl^- to form the BiOCl precipitate [reaction (3)], which further reacts with VO_3^- to form $BiVO_4$ [reaction (4)]. Both $BiVO_4$ and BiOCl are present in the precursor, as shown in Fig. 2. In addition, the elevated temperature and pressure during the hydrothermal process may accelerate the conversion from BiOCl to $BiVO_4$. However, an incomplete

transformation can be seen, as the residual BiOCl is still present in the sample due to the excess amount of Cl^- present in the solution.

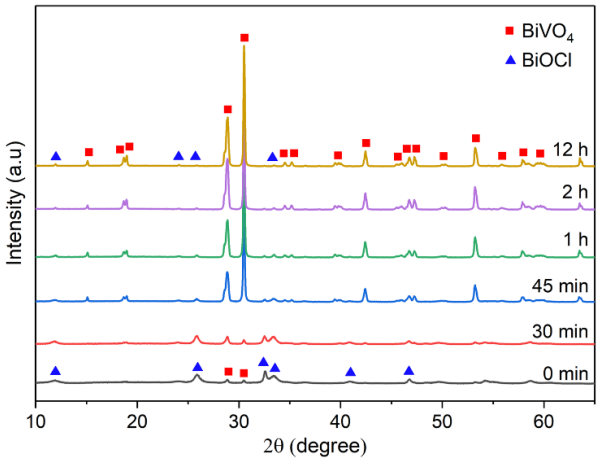

Fig. 2. XRD diffractograms of Bi3 with a different heating time of hydrothermal synthesis.

3.2. Morphology of $BiVO_4$ samples

Morphologies of $BiVO_4$ prepared with a different molar amount of KCl are depicted in SEM micrographs, as can be seen in Fig. 3. A rod-like $BiVO_4$ (Fig. 3a) can be obtained when the synthesis is prepared without KCl. The anisotropic growth of rod-like structure may be attributed to the pH~1.8 of the precursor [9]. The shape of particles has been found to transform from polyhedron to rod-like structure due to an increase in pH value, which in turn lowers the solute concentration [9,21,26,27]. When 1 mmol of KCl is added, the $BiVO_4$ particles take a short rod-like form, as shown in Fig. 3b. As the amount of KCl further rises to 2 mmol, the rod-like $BiVO_4$ connect each other in four directions to form the four arms of a cruciate structure (Fig. 3c). Further additional amount of KCl (3 mmol) allows a suitable condition for dendritic structure with small branches grown out from four arms to assume a shuriken-like structure, as can be seen in Fig. 3d. Fig. 3e illustrates the $BiVO_4$ structure resembles a tabular block with an uneven assembly of small particles as the concentration of KCl reaches 5 mmol.

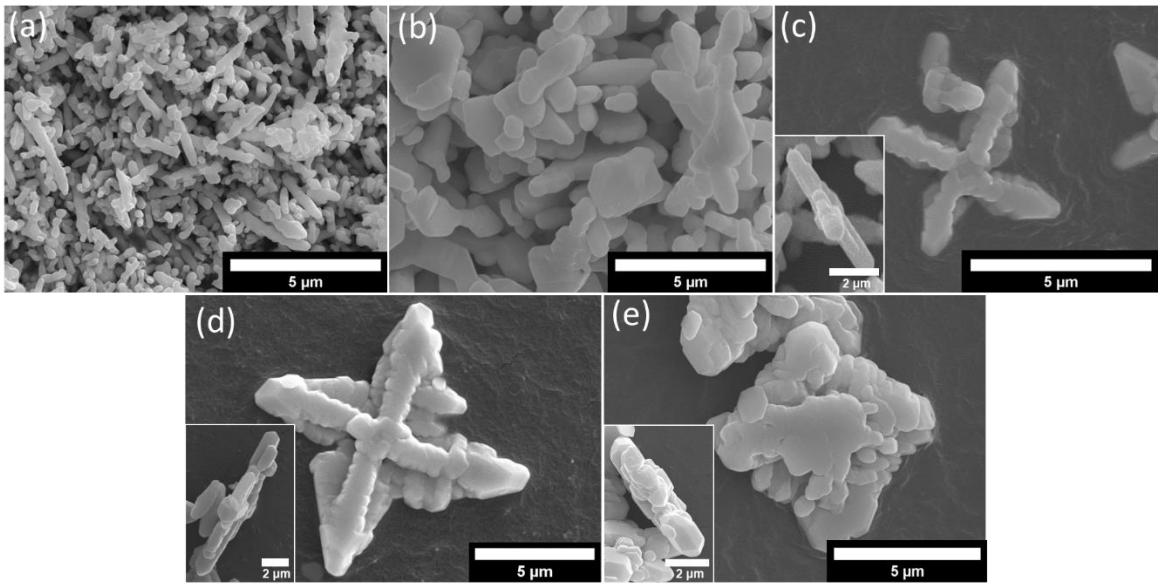

Fig. 3. FE-SEM micrographs of (a) Bi0 (0 mmol KCl) and (b) Bi1 (1 mmol KCl); and the top-view and side-view micrographs of (c) Bi2 (2 mmol KCl), (d) Bi3 (3 mmol KCl), and (e) Bi5 (5 mmol KCl).

The morphology evolution of $BiVO_4$ from rod-like structure to dendrite and then to tabular form visibly correlates with the increase in KCl concentration as depicted in Fig. 4. A similar transformation of $BiVO_4$ has been reported by Xi and coworkers [5], except that the phenomenon occurs when the acidity of the precursor is increased. It is worth mentioning that they synthesized $BiVO_4$ using $BiCl_3$ as a source of Bi^{3+}. Thus, the chemical reaction involving the BiOCl intermediate could be similar to the current study. According to this study and theirs, either increasing acidity or Cl^- concentration could provide a similar outcome of the morphological evolution of $BiVO_4$. A plausible reason is related to the solubility of BiOCl. Since BiOCl is the intermediate phase followed by its transformation into $BiVO_4$, the concentration of BiOCl in the precursor could dictate the crystal growth of $BiVO_4$ because its concentration influences the free Bi^{3+} ions, which react with VO^{3-} ions during the $BiVO_4$ formation. It is known that both H_3O^+ and Cl^- ions play a major role in the dissolution of BiOCl to form $BiCl_4^-$ through a chemical reaction (5) [28]:

$$BiO^{+} + 2H_3O^{+} + 4Cl^{-} \rightleftharpoons BiCl_4^{-} + 3H_2O \qquad (5)$$

In case of this study, the additional Cl^{-} ions (more than 1 mmol of KCl) could dissolve more BiOCl and increase the concentration of the solute in the solution, especially $BiCl_4^{-}$ ions. The detailed calculation of the $BiCl_4^{-}$ concentration, corresponding to Cl^{-} content in the precursor, is included in the Supplementary Information.

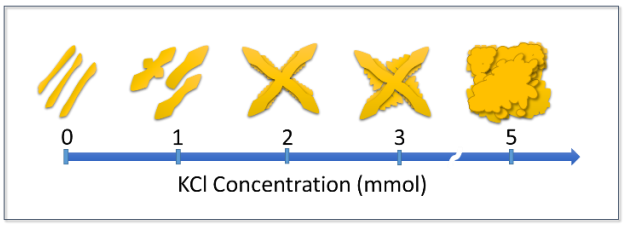

Fig. 4. Schematic illustration of the morphological development of as-prepared $BiVO_4$ respective to the KCl concentration in the precursor.

The morphology of $BiVO_4$ can be explained as follows. The BiOCl precipitates during the preparation stage due to homogeneous nucleation. Its growth rate is relatively slow as they take the form of nanoparticles, as shown in Fig. S2a (Supplementary Information). At 1 mmol addition of KCl, the number of particles of BiOCl is large. Also, the concentration of free Bi^{3+} ions in the solution is substantially low, leading to difficulty in the nucleation of $BiVO_4$. Thus, the formation and growth of the $BiVO_4$ crystals mainly depend on the transformation from BiOCl to $BiVO_4$ via the reaction with VO_3^{-}. As the concentration of KCl is increased, the number of BiOCl particles decreases, and more free Bi^{3+} ions are generated. Since the homogeneous nucleation of $BiVO_4$ is rather difficult, the $BiVO_4$ particles transform from the BiOCl particles and can grow larger in volume by the reaction between the free Bi^{3+} and VO_3^{-} ions. As a result, raising concentration of KCl leads to different morphologies of the samples, as depicted in Fig. 3c-e. It is worth mentioning that the shuriken-like $BiVO_4$ (the dendritic structure) in Fig. 3d can be obtained with the addition of

3 mmol KCl. The directional growth of the $BiVO_4$ crystals may be attributed to the variation in the relative growth rate of each crystal facet. Additionally, the dendrite $BiVO_4$ tends to have a crystal preferential growth in the [001] direction [29–31] due to the high surface energy of {001} facets [32]. The detailed morphological evolution of the shuriken-like $BiVO_4$ (Bi3) at different stages of the hydrothermal route and the additional SEM micrograph (Fig. S2) are given in the Supplementary Information.

In addition to the role of the BiOCl formation and its dissolution, the Cl^- ions also decrease the surface energy and stabilize {010} facets of $BiVO_4$ during the hydrothermal synthesis [15]. Therefore, it is understandable that $BiVO_4$ has the preferential growth in a 2D plane along the {010} planes with a smooth surface as the concentration of Cl^- increases. The preferential growth along the {010} planes in relation to the concentration of Cl^- ion is consistent with the XRD result.

3.3. Optical absorption properties of the as-prepared samples

Absorption properties of as-synthesized samples were evaluated by UV-Vis diffuse reflectance spectra. Fig. 5a shows absorption spectra of the samples, converted from reflectance data of the samples using Kubelka-Munk equation, $F(R) = (1-R)^2/2R$, where F(R) and R are Kubelka-Munk function and reflectance, respectively. It is observed that the absorption edge of $BiVO_4$ has a redshift correlating with the increase in the content of KCl, which is consistent with the color of $BiVO_4$ as it changes from yellow to orange. It indicates $BiVO_4$ samples prepared with higher KCl content can absorb a broader wavelength of visible light. However, there is no significant difference in absorption edge of the sample after further addition of KCl content from 3 mmol (Bi3) to 5 mmol (Bi5), as shown in Fig. 5a.

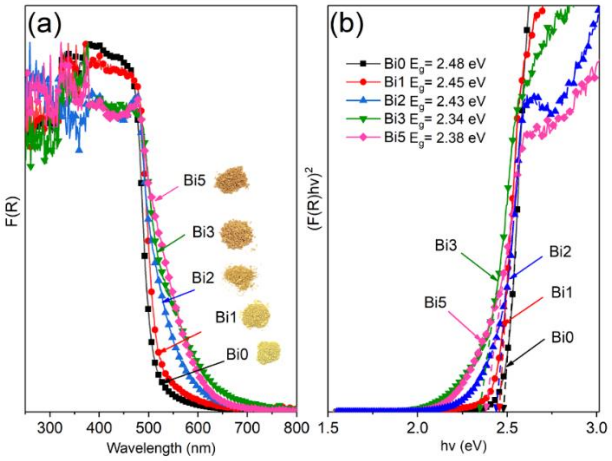

Fig. 5. (a) UV-Vis absorption spectra and (b) Tauc plot of $BiVO_4$ with a different amount of KCl.

Bandgap of each sample is determined using the following equation Eq (1) [10,33,34]:

$$\alpha h\upsilon = A(h\upsilon - E_g)^{n/2} \qquad (1)$$

where α is absorption coefficient, hυ is the photon energy, A is a constant associated with the material, and E_g is the bandgap (eV). The α can be replaced by F(R) in the Tauc plot to estimate the bandgap. As $BiVO_4$ is a direct transition semiconductor, thus the integer n = 1 is used in Eq (1). Therefore, $(F(R)hv)^2$ is plotted against hυ, as illustrated in Fig. 5b, where the bandgap of the samples can be estimated by extrapolating the linear part of the curve to intercept x-axis. The estimated E_g values of the samples are listed in Table 1. The Bi0 has E_g value of 2.48 eV, which is similar to a previous report [10]. Interestingly, the E_g value of the sample is decreased as the KCl content rises, indicating that the addition of KCl in the precursor influences on the optical absorption properties of $BiVO_4$. Unlike absorption spectra, the Tauc plot (Fig.5(b)) visibly reveals that the E_g value of Bi3 (2.34 eV) is narrower than that of Bi5 (2.38 eV). Therefore, E_g values of the $BiVO_4$ sample follow the order of Bi0 > Bi1 > Bi2 > Bi5 > Bi3.

The current finding differs from prior studies [6,15], which reported that the concentration of Cl^- from NaCl and $TiCl_3$ had no obvious effect on the absorption edge and bandgap value of the $BiVO_4$

sample. It could be ascribed to the different conditions of synthesis, in which Cl^- was added in different orders. Both previous studies added the Cl^- after NH_4VO_3 when $BiVO_4$ could have already formed, whereas Cl^- in this study was introduced before NH_4VO_3 addition. In order to confirm this, two $BiVO_4$ samples with 3 mmol of KCl were prepared using the same procedure as in the present study, except for changing the order of adding KCl to the precursor. The absorption spectra of the samples are shown in Fig S3 (Supplementary Information). When Cl^- was introduced into the precursor after NH_4VO_3, the absorption spectra of the sample have no significant difference from that of the sample without KCl, which is consistent with the previous studies [6,15]. It could be said that if Cl^- was added after NH_4VO_3, the tetragonal zircon-type $BiVO_4$ intermediate already formed due to its low formation temperature [7]. Thus, the sample prepared with KCl addition after NH_4VO_3, in a sense, goes through a similar formation process as the one without KCl addition. On the other hand, the sample prepared with KCl addition before NH_4VO_3 would go through a different formation route, in which the monoclinic $BiVO_4$ transformed from BiOCl intermediate, as revealed in XRD patterns in Fig. 2. To further confirm this, pure BiOCl powder (1 mmol) was used as a starting material with the addition of KCl (2 mmol) in a solution with a pH value of 1.8 to simulate the preparation of the Bi3 sample. The results demonstrate that the absorption spectrum (Fig. S3, Supplementary Information) and the XRD patterns (Fig. S4, Supplementary Information) of the $BiVO_4$ sample prepared using pure BiOCl as a Bi^{3+} source are indeed similar to those of the Bi3 sample prepared with KCl addition before NH_4VO_3. Therefore, the reduction in bandgap may be attributed to the defect in the $BiVO_4$ crystal structure after the conversion from BiOCl.

3.4. X-ray photoelectron spectroscopy (XPS)

Elemental composition and chemical state of various samples were analyzed using XPS spectra. In Fig. 6a, the XPS survey spectra of the as-synthesized Bi0, Bi3, and Bi5 samples confirmed the presence of Bi, V, and O elements. Fig. 6b shows two peaks located at 164.6 and 159.3 eV, which

are assigned to Bi $4f_{5/2}$ and Bi $4f_{7/2}$, respectively. In Fig. 6c, the V $2p_{1/2}$ (524.4 eV) and V $2p_{3/2}$ (516.8 eV) spectra of V 2p orbitals correspond to V−O bonds, indicating the existence of V^{5+} in the samples [35]. Fig. 6d displays O 1s spectra with a peak at 530 eV, assigned to the bonding with the lattice oxygen (Bi−O) of $BiVO_4$ [34,36–38]. Based on high-resolution XPS spectra, the different amount of KCl has no significant influence on the chemical state of $BiVO_4$. However, a small amount of Cl is detected for $BiVO_4$ prepared with additional KCl (Bi3 and Bi5). In Fig. 6e, two spin orbital peaks of Bi3 located at 199.5 and 198.2 eV, respectively, associate with Cl $2p_{1/2}$ and Cl $2p_{3/2}$ of Cl^- in BiOCl [36]. Whereas, the Cl 2p orbital peaks of the Bi5 sample exhibit a slight blueshift to 200.3 and 198.6 eV, respectively, when KCl and BiOCl content is increased. The small amount of BiOCl in the sample observed in the XPS analysis is in accordance with the XRD result (Fig.1).

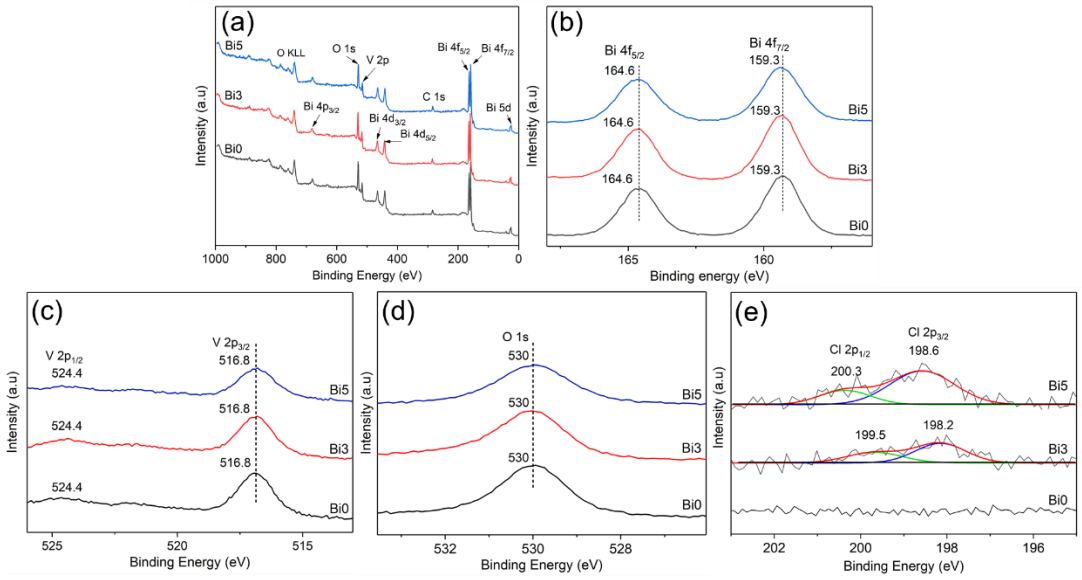

Fig. 6. (a) XPS survey spectra of $BiVO_4$ samples and high-resolution XPS spectra of (b) Bi 4f, (c) V 2p, (d) O 1s, and (e) Cl 2p.

3.5. Photocatalytic activities of the samples

Photocatalytic activities of the as-synthesized $BiVO_4$ with different concentrations of KCl were evaluated by plotting the photodegradation of RhB (C_t/C_0) against irradiation time (t), as shown in Fig. 7. To determine the stability of the RhB solution in the test condition, a photolysis of the blank RhB solution was conducted without any photocatalyst. Fig. 7 illustrates the photolysis of the blank RhB solution showed no significant decrease in concentration over 240 min, implying RhB solution remained stable in this photocatalytic test condition. Under the same condition, the concentration of all RhB solutions containing the photocatalyst was drastically reduced over time. After 240 min of irradiation, the Bi3 sample exhibited the highest photocatalytic performance as about 94.7% of RhB was degraded. It was followed by Bi2 (93.4%) with only a slight difference. Whereas, Bi5 only degraded about 63.9% of RhB, which demonstrated the lowest photocatalytic activity among the samples. The temporal absorption spectra of RhB solution in the presence of each sample are shown in Fig. S5 (Supplementary Information).

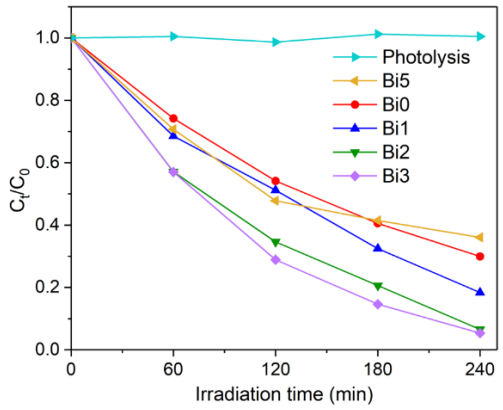

Fig. 7. Photodegradation of RhB solution without any photocatalyst and with $BiVO_4$ samples prepared with a different amount of KCl under visible light ($\lambda > 420$ nm).

To further study and compare the photocatalytic performance of the samples, photodegradation rate constants were determined utilizing a pseudo-first-order reaction equation as in Eq. (2):

$$\ln(C_0/C_t) = kt \qquad (2)$$

where, C_0, C_t, k, and t are initial concentration, concentration at a given time, photodegradation rate constants, and irradiation time, respectively. The values of k obtained from $\ln(C_0/C_t)$ vs. kt plot in Fig. 8a are also listed in Table 1. With the use of the specific surface area of each sample (S_{BET} in Table 1), the photodegradation rate k per specific surface area (k/S_{BET}) is used to compare the photocatalytic degradation of RhB for each sample.

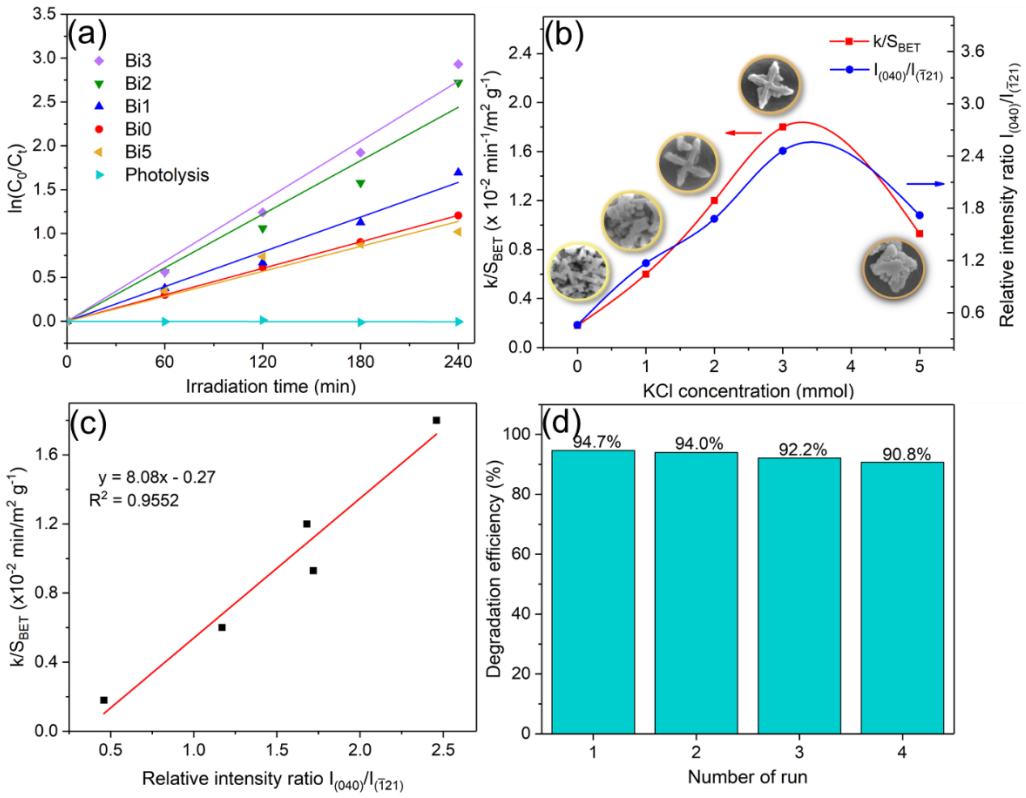

Fig. 8. (a) Pseudo-first-order kinetic degradation of RhB by $BiVO_4$ prepared with a different amount of KCl precursor; (b) Variation of both photocatalytic degradation rate constant (k) over S_{BET} (k/S_{BET}) and relative intensity ratio $I_{(040)}/I_{(\bar{1}21)}$ with respect to the KCl concentration in precursor; (c) Linear relationship between k/S_{BET} and relative intensity ratio $I_{(040)}/I_{(\bar{1}21)}$; and (d) Reusability test of the Bi3 sample for RhB degradation over four cycles under visible light ($\lambda > 420$ nm).

Fig. 8b demonstrates the relationship between k/S_{BET} and relative intensity ratio $I_{(040)}/I_{(\bar{1}21)}$ with respect to the concentration of KCl. The k/S_{BET} value surges along with the $I_{(040)}/I_{(\bar{1}21)}$ ratio when

KCl content is increased until it reaches around 3 mmol, and then goes down when it reaches 5 mmol. Both the k/S_{BET} values and the $I_{(040)}/I_{(\bar{1}21)}$ ratios follow a very similar trend, and they can be used to create a linear relationship between both of them, as plotted in Fig. 8c. Based on the figure, it indicates the dependency of k/S_{BET} on the intensity ratio $I_{(040)}/I_{(\bar{1}21)}$ of the samples. It is commonly known that a combination of various aspects, such as morphology, bandgap, crystal structure, and specific surface area, influences the photocatalytic performance of photocatalysts. Based on the results in this study, the relative intensity ratio $I_{(040)}/I_{(\bar{1}21)}$ plays a major role in the enhanced photocatalytic degradation of the RhB dye. The increase in the $I_{(040)}/I_{(\bar{1}21)}$ intensity ratio associates with the enhanced exposure of {010} facets, promoting the photocatalytic activity of the $BiVO_4$ [2,5,6,10–12]. The Bi3 sample (KCl = 3 mmol) with a shuriken-like structure exhibits the highest RhB photodegradation ascribed to the highest relative intensity ratio $I_{(040)}/I_{(\bar{1}21)}$. The narrowest bandgap of the Bi3 sample among the samples may also contribute, to some extent, to the enhancement of the photocatalytic performance as it could provide superior visible-light absorption. Based on the above experimental results and analyses, it could be concluded the KCl concentration is a key factor that influences, via modification of the reaction path, the crystal growth, crystal structure, morphology, and optical property of $BiVO_4$, which in turn affect the photocatalytic performance of $BiVO_4$.

Reusability test was conducted for the Bi3 sample in order to study its stability. The test was repeatedly run for fours cycles under identical condition. After each cycle, the photocatalyst was collected via centrifuge and put in a fresh RhB solution for another run. Fig. 8d shows that the Bi3 sample exhibits good stability, as RhB degradation efficiency of the Bi3 sample only decreases slightly from 94.7% to 90.8% after four cycles. A loss of photocatalyst during recovery process might contribute to the reduction in RhB degradation efficiency. Moreover, there is no significant

change in the crystal structure of the Bi3 sample after irradiation for four cycles, based on XRD result in Fig. S6 (Supplementary Information).

4. Conclusion

The $BiVO_4$ samples with different morphologies were synthesized using a varied amount of KCl in the hydrothermal synthesis. The concentration of Cl^- ions from KCl played a major role in the crystal growth of $BiVO_4$ due to the formation of BiOCl intermediate and the order of the KCl addition that altered the intermediate phase, which influenced the final morphology of the $BiVO_4$. The shuriken-like $BiVO_4$ (Bi3) with 3 mmol of KCl exhibits the highest photocatalytic performance for RhB degradation among the as-synthesized samples owing to the high relative intensity ratios of $I_{(040)}/I_{(\bar{1}21)}$ and the narrow bandgap. The present work contributes to the development of various dye degradation systems. Our findings provide an important clue into the effect of Cl^- concentration on BiOCl intermediate, influencing the crystal growth, absorption property, and morphology as well as the photocatalytic performance of $BiVO_4$.

Conflicts of interest

There are no conflicts to declare.

Acknowledgements

The authors thank to Japan International Cooperation Agency (JICA) for AUN/SEED-Net scholarship program.

Reference

[1] H.L. Tan, R. Amal, Y.H. Ng, Alternative strategies in improving the photocatalytic and photoelectrochemical activities of visible light-driven BiVO4: A review, J. Mater. Chem. A. 5 (2017) 16498–16521. https://doi.org/10.1039/c7ta04441k.

[2] S.M. Thalluri, M. Hussain, G. Saracco, J. Barber, N. Russo, Green-synthesized BiVO4 oriented along {040} facets for visible-light-driven ethylene degradation, Ind. Eng. Chem. Res. 53 (2014) 2640–2646. https://doi.org/10.1021/ie403999g.

[3] M. Hojamberdiev, G. Zhu, Z.C. Kadirova, J. Han, J. Liang, J. Zhou, X. Wei, P. Liu, Morphology-controlled growth of BiVO4 crystals by hydrothermal method assisted with ethylene glycol and ethylenediamine and their photocatalytic activity, Mater. Chem. Phys. 165 (2015) 188–195. https://doi.org/10.1016/j.matchemphys.2015.09.015.

[4] T. Senasu, S. Youngme, K. Hemavibool, S. Nanan, Sunlight-driven photodegradation of oxytetracycline antibiotic by BiVO4 photocatalyst, J. Solid State Chem. 297 (2021) 122088. https://doi.org/10.1016/j.jssc.2021.122088.

[5] G. Xi, J. Ye, Synthesis of bismuth vanadate nanoplates with exposed {001} facets and enhanced visible-light photocatalytic properties, Chem. Commun. 46 (2010) 1893–1895. https://doi.org/10.1039/b923435g.

[6] D. Wang, H. Jiang, X. Zong, Q. Xu, Y. Ma, G. Li, C. Li, Crystal facet dependence of water oxidation on BiVO4 sheets under visible light irradiation, Chem. - A Eur. J. 17 (2011) 1275–1282. https://doi.org/10.1002/chem.201001636.

[7] A. Kudo, K. Omori, H. Kato, A novel aqueous process for preparation of crystal form-controlled and highly crystalline BiVO4 powder from layered vanadates at room temperature and its photocatalytic and photophysical properties, J. Am. Chem. Soc. 121 (1999) 11459–11467. https://doi.org/10.1021/ja992541y.

[8] S. Tokunaga, H. Kato, A. Kudo, Selective preparation of monoclinic and tetragonal BiVO4 with scheelite structure and their photocatalytic properties, Chem. Mater. 13 (2001) 4624–4628. https://doi.org/10.1021/cm0103390.

[9] Y. Zhao, R. Li, L. Mu, C. Li, Significance of crystal morphology controlling in semiconductor-based photocatalysis: a case study on BiVO4 photocatalyst, Cryst. Growth Des. 17 (2017) 2923–2928. https://doi.org/10.1021/acs.cgd.7b00291.

[10] G. Zhao, W. Liu, Y. Hao, Z. Zhang, Q. Li, S. Zang, Nanostructured shuriken-like BiVO4 with preferentially exposed {010} facets: Preparation, formation mechanism, and enhanced photocatalytic performance, Dalt. Trans. 47 (2018) 1325–1336. https://doi.org/10.1039/c7dt04431c.

[11] Y. Li, Z. Sun, S. Zhu, Y. Liao, Z. Chen, D. Zhang, Fabrication of BiVO4 nanoplates with active facets on graphene sheets for visible-light photocatalyst, Carbon N. Y. 94 (2015) 599–606. https://doi.org/10.1016/j.carbon.2015.07.042.

[12] L. Xia, J. Li, J. Bai, L. Li, S. Chen, B. Zhou, BiVO4 photoanode with exposed (040) facets for enhanced photoelectrochemical performance, Nano-Micro Lett. 10 (2018) 1–10. https://doi.org/10.1007/s40820-017-0163-3.

[13] B. Baral, K. Parida, {040/110} Facet isotype heterojunctions with monoclinic scheelite BiVO4, Inorg. Chem. (2020). https://doi.org/10.1021/acs.inorgchem.0c01465.

[14] X. Yu, V. V. Ordomsky, A.Y. Khodakov, Selective deposition of cobalt and copper oxides on BiVO4 facets for enhancement of CO2 photocatalytic reduction to hydrocarbons, ChemCatChem. 12 (2020) 740–749. https://doi.org/10.1002/cctc.201901115.

[15] S. Xie, Z. Shen, H. Zhang, J. Cheng, Q. Zhang, Y. Wang, Photocatalytic coupling of formaldehyde to ethylene glycol and glycolaldehyde over bismuth vanadate with controllable facets and cocatalysts, Catal. Sci. Technol. 7 (2017) 923–933. https://doi.org/10.1039/c6cy02510b.

[16] G. Zhao, W. Liu, J. Li, Q. Lv, W. Li, L. Liang, Facile synthesis of hierarchically structured BiVO 4 oriented along (010) facets with different morphologies and their photocatalytic properties, Appl. Surf. Sci. 390 (2016) 531–539. https://doi.org/10.1016/j.apsusc.2016.08.126.

[17] B. Xu, A. Zada, G. Wang, Y. Qu, Boosting the visible-light photoactivities of BiVO4 nanoplates by Eu doping and coupling CeO:X nanoparticles for CO2 reduction and organic oxidation, Sustain. Energy Fuels. 3 (2019) 3363–3369. https://doi.org/10.1039/c9se00409b.

[18] S.W. Cao, Z. Yin, J. Barber, F.Y.C. Boey, S.C.J. Loo, C. Xue, Preparation of Au-BiVO4 heterogeneous nanostructures as highly efficient visible-light photocatalysts, ACS Appl. Mater. Interfaces. 4 (2012) 418–423. https://doi.org/10.1021/am201481b.

[19] X. Zhu, F. Zhang, M. Wang, X. Gao, Y. Luo, J. Xue, Y. Zhang, J. Ding, S. Sun, J. Bao, C. Gao, A shuriken-shaped m-BiVO 4 /{0 0 1}-TiO 2 heterojunction: Synthesis, structure and enhanced visible light photocatalytic activity, Appl. Catal. A Gen. 521 (2016) 42–49. https://doi.org/10.1016/j.apcata.2015.10.017.

[20] D. Diemente, Why is bismuth subchloride soluble in acid?, J. Chem. Educ. 74 (1997) 398–399. https://doi.org/10.1021/ed074p398.

[21] G. Tan, L. Zhang, H. Ren, S. Wei, J. Huang, A. Xia, Effects of pH on the hierarchical structures and photocatalytic performance of BiVO4 powders prepared via the microwave hydrothermal method, ACS Appl. Mater. Interfaces. 5 (2013) 5186–5193. https://doi.org/10.1021/am401019m.

[22] A. Ajmal, I. Majeed, R.N. Malik, H. Idriss, M.A. Nadeem, Principles and mechanisms of photocatalytic dye degradation on TiO2 based photocatalysts: a comparative overview, RSC Adv. 4 (2014) 37003–37026. https://doi.org/10.1039/c4ra06658h.

[23] K. Iqbal, A. Iqbal, A.M. Kirillov, B. Wang, W. Liu, Y. Tang, A new Ce-doped MgAl-LDH@Au nanocatalyst for highly efficient reductive degradation of organic contaminants, J. Mater. Chem. A. 5 (2017) 6716–6724. https://doi.org/10.1039/C6TA10880F.

[24] K. Iqbal, A. Iqbal, A.M. Kirillov, W. Liu, Y. Tang, Hybrid metal-organic-framework/inorganic nanocatalyst toward highly efficient discoloration of organic dyes in aqueous medium, Inorg. Chem. 57 (2018) 13270–13278. https://doi.org/10.1021/acs.inorgchem.8b01826.

[25] P. Singh, A. Borthakur, P.K. Mishra, D. Tiwary, Nano-materials as photocatalysts for degradation of environmental pollutants: challenges and possibilities, Elsevier, 2019.

[26] P. McFadyen, E. Matijević, Copper hydrous oxide sols of uniform particle shape and size, J. Colloid Interface Sci. 44 (1973) 95–106. https://doi.org/10.1016/0021-9797(73)90196-3.

[27] Y. Sui, W. Fu, H. Yang, Y. Zeng, Y. Zhang, Q. Zhao, Y. Li, X. Zhou, Y. Leng, M. Li, G. Zou, Low temperature synthesis of Cu2O crystals: Shape evolution and growth mechanism, Cryst. Growth Des. 10 (2010) 99–108. https://doi.org/10.1021/cg900437x.

[28] M.N. Ackermann, Why is Bismuth Subchloride Soluble in Acid?, J. Chem. Educ. 75 (1998) 523. https://doi.org/10.1021/ed075p523.

[29] D. Li, W. Shi, W. Zheng, Controlled synthesis of m-BiVO4 dendrites for enhanced photocatalytic activity, J. Cryst. Growth. 448 (2016) 93–96. https://doi.org/10.1016/j.jcrysgro.2016.05.028.

[30] L. Zhou, W. Wang, H. Xu, Controllable synthesis of three-dimensional well-defined BiVO4 mesocrystals via a facile additive-free aqueous strategy, Cryst. Growth Des. 8 (2008) 728–733. https://doi.org/10.1021/cg0705761.

[31] S.S. Patil, D.P. Dubal, V.G. Deonikar, M.S. Tamboli, J.D. Ambekar, P. Gomez-Romero, S.S. Kolekar, B.B. Kale, D.R. Patil, Fern-like rGO/BiVO4 hybrid nanostructures for high-energy symmetric supercapacitor, ACS Appl. Mater. Interfaces. 8 (2016) 31602–31610. https://doi.org/10.1021/acsami.6b08165.

[32] G.L. Li, First-principles investigation of the surface properties of fergusonite-type monoclinic BiVO4 photocatalyst, RSC Adv. 7 (2017) 9130–9140. https://doi.org/10.1039/c6ra28006d.

[33] S. Sun, W. Wang, L. Zhou, H. Xu, Efficient methylene blue removal over hydrothermally synthesized starlike BiVO4, Ind. Eng. Chem. Res. 48 (2009) 1735–1739. https://doi.org/10.1021/ie801516u.

[34] D.P. Jaihindh, B. Thirumalraj, S.M. Chen, P. Balasubramanian, Y.P. Fu, Facile synthesis of hierarchically nanostructured bismuth vanadate: An efficient photocatalyst for degradation and detection of hexavalent chromium, J. Hazard. Mater. 367 (2019) 647–657. https://doi.org/10.1016/j.jhazmat.2019.01.017.

[35] T. Senasu, S. Youngme, K. Hemavibool, S. Nanan, Sunlight-driven photodegradation of oxytetracycline antibiotic by BiVO4 photocatalyst, J. Solid State Chem. 297 (2021) 122088. https://doi.org/10.1016/j.jssc.2021.122088.

[36] C. Feng, D. Wang, B. Jin, Z. Jiao, The enhanced photocatalytic properties of BiOCl/BiVO4 p-n heterojunctions via plasmon resonance of metal Bi, RSC Adv. 5 (2015) 75947–75952. https://doi.org/10.1039/c5ra13886h.

[37] M. Zhu, Q. Liu, W. Chen, Y. Yin, L. Ge, H. Li, K. Wang, Boosting the visible-light photoactivity of BiOCl/BiVO4/N-GQD ternary heterojunctions based on internal Z-scheme charge transfer of N-GQDs: simultaneous band gap narrowing and carrier lifetime prolonging, ACS Appl. Mater. Interfaces. 9 (2017) 38832–38841. https://doi.org/10.1021/acsami.7b14412.

[38] L. Zhang, Q. Luo, X. Chen, M.S. Tse, O.K. Tan, K.H.H. Li, Y.Y. Tay, C.K. Lim, X. Guo, H. holden, Mechanochemically synthesized CuO/m-BiVO4 composite with enhanced photoelectrochemical and photocatalytic properties, RSC Adv. 6 (2016) 65038–65046. https://doi.org/10.1039/c6ra13411d.